Ground state structures in ferrofluid monolayers

Taisia A. Prokopieva,[1] Victor A. Danilov,[1] Sofia S. Kantorovich,[1,2] and Christian Holm[2]
[1]*Urals State University 51 Lenin Ave, Ekaterinburg 620083, Russia*
[2]*Institut fur Computerphysik Universitat Stuttgart Pfaffenwaldring 27, 70569 Stuttgart, Germany*
(Received 21 May 2009; published 29 September 2009)

A combination of analytical calculations and Monte Carlo simulations is used to find the ground state structures in monodisperse ferrofluid monolayers. Taking into account the magnetic dipole-dipole interaction between all particles in the system we observe different topological structures that are likely to exist at low temperatures. The most energetically favored structures we find are rings, embedded rings, and rings side by side, and we are able to derive analytical expressions for the total energy of these structures. A detailed analysis of embedded rings and rings side by side shows that the interring interactions are negligible. We furthermore find that a single ideal ring is the ground state structure for a ferrofluid monolayer. We compared our theoretical predictions to the results of simulated annealing data and found them to be in excellent agreement.

DOI: 10.1103/PhysRevE.80.031404 PACS number(s): 82.70.−y, 61.20.Gy, 61.20.Ja, 75.50.Mm

I. INTRODUCTION

Since their synthesis in 1964 [1] suspensions of magnetic nanoparticles (diameters of the magnetic core: ~10–50 nm) in nonmagnetic carrier liquids have been called magnetic fluids (ferrofluids, ferrocolloids), and their investigation has become an independent branch of science.

Particles in ferrofluids are made of Fe, Co, Ni, and their oxides. The size of the magnetic particle is smaller than the critical size of the monodomain state for the latter ferromagnetic and antiferromagnetic materials. So, each particle is homogeneously magnetized and possesses a magnetic moment proportional to the particle volume and the saturation magnetization of the bulk material. For nonelectrolyte carrier liquids a steric coating of magnetic cores is used to prevent the coagulation, with an oleic acid (commonly) taken as a stabilizer [2]. Strong response to an external magnetic field, represented by ferrocolloids in combination with a liquid state, gives rise to numerous applications of magnetic fluids in engineering and natural science. Functionalized magnetic fluids are used as an effective drug carrier tool and can be used also in cancer treatment (e.g., hyperthermia) [3,4].

Despite the active research carried out in the field of cluster formation in magnetic fluids (see, for instance, [5–29]) their complex microstructure remains a stumbling block for both experimentalists and theorists. The nanosized clusters in opaque carriers are difficult to be seen; the long range character of the magnetic interactions and the essential polydispersity of particles in ferrofluids make their analytical description challenging. Thin films and monolayers recently became a more successful experimental scenario to assert the existence of the aggregation process [30–33]. In the experiments of Philipse and co-workers [32,33], images obtained by cryogenic transmission electron microscopy gave ample evidence of the existence of chainlike and ringlike structures in ferrofluid monolayers, where all particles are trapped in one plane but their magnetic moments are free to fluctuate in three dimensions [quasi-two-dimensional (q2D) monolayers]. Also the theoretical and simulation analysis of cluster formation in ferrofluid monolayers is now available [34]. However, monolayer studies gave rise to numerous questions about the influence the geometry has on the interparticle interactions and on the entropy. In order to understand the peculiarities brought by the q2D geometry better, we present a study of ground state structures in ferrofluid monolayers. This question was addressed several times in literature in the works [35–39], for instance, but neither consistent approach nor detailed analysis of the possible ground state structures was presented.

One of the reasons for lacking a complete picture of ground state structures is that, on the one hand, for complex energy landscapes like the ones dictated by dipolar interactions it is very difficult to get precise ground state structures via simulations and, on the other hand, the analytical treatment of many-body problems also seems to be impossible. The aim of the present study is to develop an approach which avoids this complexity but still provides reliable and well-founded results. The main idea which served as a starting point for this paper was the following:

(1) We used simulated annealing in a system of ferroparticles in a monolayer moderately slow, but we repeated the simulation sufficiently many times in order to see if some structural motives dominate.

(2) We analyzed the most frequent structures and classified them.

(3) For some classified topologies we constructed analytical expressions for the energy and minimized them in order to fulfill *the main goal of this paper*, i.e., to find the topology of the ferroparticle structure in a monolayer at $T=0$ K with the lowest energy.

The structure of this paper is the following. In Sec. II we describe our used methods to perform computer experiments and present the simulation results. For the structures found in the simulations we construct analytic expressions of the energy in Sec. III. Section IV is dedicated to the discussion of the most probable ground state structures. In Sec. IV, we perform a comparison of the analytical results to the predictions of our simulations. The discussions and main results are summarized in Sec. V.

II. SIMULATION DETAILS

Simulations of physical systems at low temperature (especially when approaching the ground state) pose a serious

problem for any simulation method due to the slow relaxation times encountered and the possible rugged or nonunique ground state structure of many complex systems. We aimed neither at running extra long simulations nor at reaching a global ground state. We describe in the following the idea behind our computer investigations and provide a brief scheme of the employed simulation technique.

Two interactions were used to model the system of monodisperse ferroparticles in a monolayer. The magnetic dipole-dipole interaction between particle magnetic moments $\mathbf{m}_i$ and $\mathbf{m}_j$ has the following form:

$$U_{dd}(ij) = -\frac{\mu_0}{4\pi}\left[3\frac{(\mathbf{m}_i\cdot\mathbf{r}_{ij})(\mathbf{m}_j\cdot\mathbf{r}_{ij})}{r^5} - \frac{(\mathbf{m}_i\cdot\mathbf{m}_j)}{r^3}\right],$$

$$\mathbf{r}_{ij} = \mathbf{r}_i - \mathbf{r}_j, \tag{1}$$

where $\mathbf{r}_{ij}=\mathbf{r}_i-\mathbf{r}_j$ is the displacement vector of two particles i and j, $\mathbf{r}_{ij}=\mathbf{r}$ and $\mu_0=4\pi\times10^{-7}$ H/m is the vacuum magnetic permeability. The pair potential in Eq. (1) is anisotropic and favors head-to-tail positions of two magnetic moments. The modulus of the particle magnetic moment is determined by the bulk magnetization M_0 of the material and the volume of the magnetic material, namely, $m=|\mathbf{m}_i|=\pi M_0(d_m)^3/6$, where d_m is the diameter of the magnetic core.

The steric repulsion can be described in terms of a standard Weeks-Chandler-Andersen potential [40],

$$U_{\mathrm{WCA}}(ij) = \begin{cases} 4\varepsilon\left[\left(\dfrac{d_m}{r_{ij}}\right)^{12} - \left(\dfrac{d_m}{r_{ij}}\right)^{6}\right] + \varepsilon, & r_{ij} < d_c \\ 0, & r_{ij} > d_c. \end{cases} \tag{2}$$

The potential is cut off at the minimum, yielding a radius $d_c=(d_m)2^{1/6}$. In principle one could also use a hard sphere potential to describe the ground state structures, but we expect no serious differences in the structures.

The simulations employed a standard Metropolis algorithm [41], and we used a dimensionless distance and energy, respectively, normalized to the units of the particle magnetic diameter d_m and the Lennard-Jones energy parameter ε. As a result, the following three dimensionless variables were used in simulations: the reduced particle diameter $\widetilde{d}_m=1$; the reduced temperature $\widetilde{T}=kT/\varepsilon$, where k is a Boltzmann constant; and finally, to make the dipolar interaction dimensionless, we introduce the factor m^2/ε, $m=(d_m)^3M_0\pi/6$ taking into account that $d_m=1$, and in this case the magnetic moments are simply unit vectors.

The probability for the Metropolis algorithm to accept a new configuration is

$$\exp(-\Delta[\widetilde{U}_{dd}+\widetilde{U}_{\mathrm{WCA}}]/\widetilde{T}).$$

Each computer experiment was organized as follows: first the system was equilibrated (until energies stayed within 5% of the average, the averaging was performed every 100 steps, the number of steps depends on the number of particles and temperature and in this case had an upper value of 2 000 000 accepted iterations) at some initial temperature $\widetilde{T}$ and then we decreased it by the value δT. The system was again equilibrated, and we tried another quench to a lower temperature until value $m^2/kT=64$ was reached. The shifts for coordinates were chosen as random numbers (with uniform distribution); the vectors of magnetic moments were rotated around a randomly chosen vector in three dimensions for a random angle.

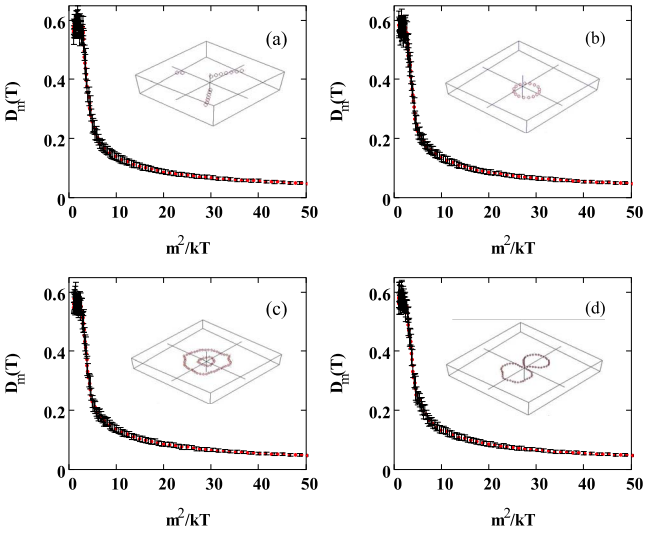

FIG. 1. (Color online) The deviation $D_m(T)$ of magnetic moments from the in-plain directions as a function of m^2/kT for the structures depicted in the legend, where we present simulation snapshots of the structures most often observed. (a) chains; (b) a single ring; (c) embedded rings; and (d) rings side by side.

The runs were started from $\widetilde{T}=1$ and $m^2/kT=4$. For this set of parameters the system of 16 ferroparticles was in a nonaggregated state. The number of steps for the preliminary equilibration was 100 000; the averaging of the energy was performed over the last 1000 steps. For different values of the temperature step δT the final cluster structures varied significantly.

Thus, in the system of 16 ferroparticles we observed

(i) for $\delta T=0.6\widetilde{T}$ short chains,

(ii) for $\delta T=0.1\widetilde{T}$ several long chains, and

(iii) for $\delta T=0.01\widetilde{T}$ a single ring.

When the number of particles was doubled (32 particles), we observed besides a chain and a ring also two embedded rings, and even two rings side by side were found for the lowest value of δT. However, a further increase in the particle number (up to 1000) did not lead to any new cluster structures. It is worth mentioning that embedded rings were also observed in the work of Morimoto and coauthors [37]. In this work they concluded that for high coupling constants and large number of particles embedded rings were the most probable structures. Below, we will investigate the question of different structure probabilities and suggest what we think is the real ground state for different numbers of particles.

The first result of this simple computer experiment was a list of cluster structures (general shapes) that were likely to be candidates for the ground state. They are presented in Figs. 1(a)–1(d): simulation snapshots of chains [Fig. 1(a)], a ring [Fig. 1(b)], embedded rings [Fig. 1(c)], and rings side by side [Fig. 1(d)].

In order to choose the ground state structure one needs to have precise values of energies for all the candidates. Al-

though the first results reduced the number of probable ground state structures from a very large number to a list of 4 only, the direct calculations were still overloaded by the particle and magnetic moment degrees of freedom. For example, from the results of our simulated annealing neither the alignment of moments nor the exact equations for the particle positions could be extracted.

Analyzing every of four general shapes we furthermore discovered that the minimum energy corresponded to the "ideal" structures. Thus, the lowest energy for a chain was reached for a rigid rodlike chain, and as for the rings, the lowest value of the energy could be achieved if rings were based on regular polygons, i.e., the centers of particles in a ring were in the vertices of regular polygons. Embedded rings and, what is a bit more surprising, rings side by side also seemed to preserve the "regularity" of basic polygons. For the latter configuration an additional series of simulation experiments was performed. The deviation of two rings side by side from the ideal structures was analyzed in terms of particle positions in the simulations. One can compute the distance between two opposite particles along the horizontal and vertical ring diameters (for an ideal ring these distances are equal to the ring diameter). In general, their ratio shows the deformation of the ring. In our simulations, it turned out that the latter ratio (between the maximum horizontal and vertical distances) in any of two rings side by side goes to unity when the temperature decreases. To estimate the fluctuations, the mean square deviation of particle positions from the radius of the ideal ring has been calculated. The value obtained is less than 1%. We also observed that with decreasing temperature the moments tend to stay within the monolayer plane. This can be seen in Figs. 1(a)–1(d), where, besides the snapshots of the structures, the simulation data for the value $D_m(T)$,

$$D_m(T) = \sqrt{\frac{\sum_{i=1}^{N} (m_z^i)^2}{\sum_{i=1}^{N} [(m_x^i)^2 + (m_y^i)^2 + (m_z^i)^2]}}, \tag{3}$$

are plotted as a function of m^2/kT. Here, m_x^i, m_y^i, and m_z^i are x, y, and z components of ith particle magnetic moment. Therefore, the magnetic moments have significantly smaller z components than their x and y ones, and the z component monotonously decreases to zero with decreasing temperature [$D_m(T)$ goes to zero when m^2/kT is larger than 10]. The simulation error bars are also plotted in the figures and do not exceed 1% for low temperatures.

This allowed us to fix the coordinates of the particles and reduce the simulation expenses significantly. On this level the number of particles in the system was varied between $N=4-100$ with a step equal to 1, $N=200-3000$ with a step equal to 100, and $N=4000-30\,000$ with a step equal to 1000. Only the rotation of moments was performed in these runs. To summarize, the simulation results provided us with a restricted number of structures corresponding to local minima in the energy landscape, and with high probability one of them corresponds to the ground state. Additionally, the spatial configurations are well defined which made it feasible to compute the energy of the candidates analytically and to compare the total energy of the structures to the results of the simulations done for fixed particle positions.

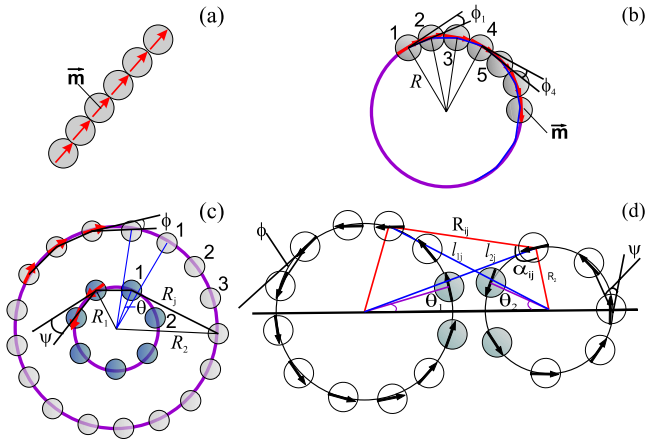

FIG. 2. (Color online) Ideal structures with notations used in the calculations. Notations are explained in the text of corresponding sections. The particle magnetic moment is denoted by m. The system under study is monodisperse. (a) a chain; (b) an ideal ring; (c) embedded rings; and (d) rings side by side.

III. ANALYTICAL EXPRESSIONS FOR THE ENERGIES

In this section we calculate total energies of different ideal structures. For notations see Figs. 2(a)–2(d). The particle magnetic moment is denoted by m and is fixed within the plain of monolayer. The system under study is monodisperse.

A. Chain

There is no need to prove that the ferroparticle chain has the minimal energy if all particles are aligned along one line together with all magnetic moments. In the ferroparticle chain of N beads there are $N-1$ interactions between the nearest neighbors with energy $-2m^2/d^3$, $N-2$ interactions of the particles separated by two diameters with energy $-2m^2/8d^3$, there are $N-3$ particles separated by three diameters, with the interaction energy $-2m^2/27d^3$, and so on. The general expression for the chain total energy $U_{CH}(N)$ has the following form:

$$U_{CH}(N) = -2\frac{m^2}{d^3}\sum_{k=1}^{N}\frac{N-k}{k^3}. \tag{4}$$

For large values of N the expression in Eq. (4) can be simplified, thus, leading to the following asymptotic behavior:

$$U_{CH}^{as}(N) = -2\frac{m^2}{d^3}\left(N\zeta(3) - \frac{\pi^2}{6}\right). \tag{5}$$

Here, $\zeta(3) \approx 1.202$ is the Riemann zeta function. This expression is very close to the one obtained in [18] [see Eq. (4), page 3050], however, the authors there had to introduce some fitting parameter, which in fact is nothing but the value of Riemann function accurately obtained above. The range of

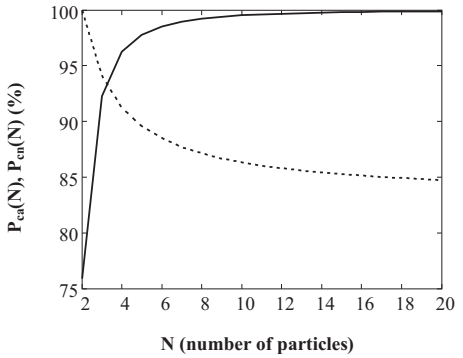

FIG. 3. The percentage deviation of the precise and asymptotic [expression (6), solid line] and precise and nearest-neighbor [expression (8), dashed line] expressions for the chain energy as functions of N (the total number of particles per chain).

validity of this approximation can be analyzed in Fig. 3, where the percentage deviation of Eq. (4) from the one given by Eq. (5) is plotted as a function of N (the total number of particles per chain) with solid line. Namely, the following ratio is plotted:

$$P_{ca}(N) = \frac{U_{CH}^{as}(N)}{U_{CH}(N)} 100. \tag{6}$$

The precision of 5% is reached already for the chain made of four particles. In other words, the asymptotic formula can safely be used to describe the energy of a chain even if the latter is relatively short. The peculiarity of Eq. (5) is that it has the same functional form as the expression for the chain energy within the approximation of the nearest-neighbor interaction, namely,

$$U_{CH}^{nn}(N) = -2\frac{m^2}{d^3}(N-1). \tag{7}$$

Both expressions consist of the product of the nearest-neighbor interaction $-2m^2/d^3$ and the linear N-dependent part. It is important to compare the usually adopted in literature approximation of the nearest neighbors to the total energy of a chain at 0 K. The expression has the form

$$P_{cn}(N) = \frac{U_{CH}^{nn}(N)}{U_{CH}(N)} 100. \tag{8}$$

The result $[P_{cn}(N)]$ is presented in Fig. 3 by dashed line. It shows the percentage deviation of the chain energy with every interaction taken into account from the chain energy calculated for the nearest neighbors only as a function of the total number of particles. It is seen that this deviation saturates and does not exceed 15% even for very long chains. The average chain length observed for commercial ferrofluids has an order of three to five particles [42]. In this length region the difference is less than 5%, which fairly validates the approximation.

B. Ideal ring

In this section we study an ideal single ring (a ring based on a regular polygon) with the radius R (from now on, we use the dimensionless radius related to the particle diameter d). The number of particles in a ring is larger than 2, $N \geq 3$. All magnetic moments are aligned in the plane of the layer. This assumption is based on the simulation results, where the magnetic moments were shown to fluctuate predominantly within the monolayer plane. As the first step on the way to find a ground state structure, we will try to pinpoint the configuration of dipoles which provides the minimal total energy for the ideal ring. For that the following model was used.

The distance a_k between the centers of particle separated by k polygon sides can be written as

$$a_k^2 = 2R^2 - 2R^2 \cos\left(\frac{2\pi k}{N}\right), \quad k = 1, \ldots, N.$$

Taking into account that ϕ_i, as it is shown in Fig. 2(b), is the angle at the ith vertex between the polygon side and the ith particle magnetic moment, $i=1,\ldots,N$, the angle between ith magnetic moment and the vector which connects ith and $(k+i)$th particles can be written as

$$\phi_i + \frac{(k-1)\pi}{N}$$

and the angle between $(i+k)$th magnetic moment and the vector which connects ith and $(k+i)$th particles has a form

$$\frac{(k+1)\pi}{N} - \phi_{i+k}.$$

Finally, the angle between ith and $(i+k)$th moments is

$$\phi_i - \phi_{i+k} + \frac{2k\pi}{N}.$$

Magnetic dipole-dipole interaction between ith and $(i+k)$th particles, thus, can be presented as follows:

$$U_{dd}(i,i+k) = \frac{m^2}{d^3 a_k^3}\left[\cos\left(\phi_i - \phi_{i+k} + \frac{2k\pi}{N}\right) - 3\cos\left(\phi_i + \frac{(k-1)\pi}{N}\right)\cos\left(\frac{(k+1)\pi}{N} - \phi_{i+k}\right)\right]. \tag{9}$$

To calculate the total ring energy at 0 K, we have to allow for every pair interaction. For this purpose, it is convenient to present the interactions in an inductive form:

(i) For $N=3$ there are N pair interactions; particles in the pairs are separated by one polygon side, we call them "one side pair interactions;"

(ii) For $N=4$ there are N one side pair interactions and $N/2$ two side pair interactions;

(iii) For $N=5$ there are N one side pair interactions, N two side pair interactions, etc.

The general expression for the total ideal ring energy is different for odd and even N.

For odd N it can be written as

$$U_R^G = \frac{m^2}{d^3}\sum_{i=1}^{N}\sum_{k=1}^{(N-1)/2}\left\{\frac{1}{a_k^3}\left[\cos\left(\phi_i - \phi_{i+k} + \frac{2\pi k}{N}\right) - 3\cos\left(\phi_i + \frac{(k-1)\pi}{N}\right)\cos\left(\frac{(k+1)\pi}{N} - \phi_{i+k}\right)\right]\right\}, \tag{10}$$

where $N+i=i$.

For even N the energy is

$$U_R^G = \frac{m^2}{d^3}\sum_{i=1}^{N}\sum_{k=1}^{N/2-1}\left\{\frac{1}{a_k^3}\left[\cos\left(\phi_i - \phi_{i+k} + \frac{2\pi k}{N}\right) - 3\cos\left(\phi_i + \frac{(k-1)\pi}{N}\right)\cos\left(\frac{(k+1)\pi}{N} - \phi_{i+k}\right)\right]\right\} + \sum_{i=1}^{N/2}\left\{\frac{1}{8R^3}\left[\cos(\phi_i - \phi_{i+N/2} + \pi) - 3\cos\left(\phi_i + \frac{(N/2-1)\pi}{n}\right)\times\cos\left(\frac{(N/2+1)\pi}{N} - \phi_{i+N/2}\right)\right]\right\}, \tag{11}$$

where $N+i=i$.

After having minimized this energy with respect to ϕ_i, we obtain the following minimum values: $\phi_i = \frac{\pi}{N} + \pi l$, $l \in \mathbb{Z}$. These values of angles mean that ferroparticle magnetic moments are aligned tangentially to the circle which an ideal ring is based on.

Having in mind that particles are in a close contact, the expression for the ideal ring energy in the ground state can be written as

$$U_R(N) = -\frac{m^2}{d^3}N\sin^3\left(\frac{\pi}{N}\right)\times\left\{\sum_{k=1}^{[(N-1)/2]}\frac{\cos\left(\frac{\pi k}{n}\right)^2 + 1}{\sin\left(\frac{\pi k}{N}\right)^3} + \frac{1}{2}\mathrm{mod}(N+1,2)\right\}. \tag{12}$$

Here, $[\cdot]$ stays for the integer part of the ratio in brackets and $\mathrm{mod}(N+1,2)$ denotes the residue of division. In the same manner we did it for a chain, the asymptotic behavior of the ring energy for large values of N can be calculated. It has the following simple form:

$$U_R^{as}(N) = -2\frac{m^2}{d^3}N\zeta(3). \tag{13}$$

The deviation of Eq. (12) from the asymptote [Eq. (13)] is presented in Fig. 4 (solid line). This expression has the form

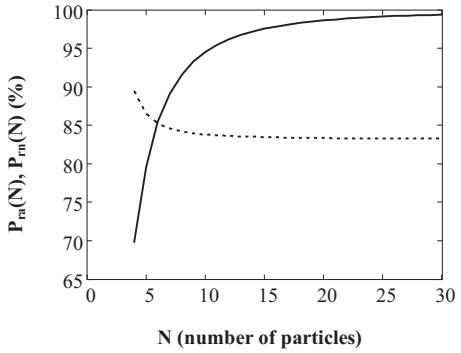

FIG. 4. The percentage deviation of the precise and asymptotic [expression (14), solid line] and precise and nearest-neighbor [expression (16), dashed line] expressions for the ideal ring energy as functions of N (the total number of particles per chain).

$$P_{ra}(N) = \frac{U_R(N)}{U_R^{as}(N)}100. \tag{14}$$

It is seen that the percentage deviation is higher than that for chains (Fig. 3, solid line), but it still becomes smaller than 5% for rings larger than ten particles. Analogously to the asymptotic chain energy presented in Eq. (5), the asymptotic ring energy has the form of a doublet energy $-2m^2/d^3$ multiplied by the linear function of N. The angle between neighboring magnetic moments is (as calculated above) $2\pi/N$, in the limit of large N and it goes to zero, and the ring becomes locally straight. This expression is close to the formula obtained by Jund and coauthors [18] [expression (5), page 3050], however, similar to the case of chain energy, it allows us to avoid the usage of fitting parameter. Here, it is also possible to compare the error of the nearest-neighbor approximation given by the following formula,

$$U_R^{nn}(N) = \frac{m^2}{d^3}N\left[\cos\left(\frac{2\pi}{N}\right) - 3\cos^2\left(\frac{\pi}{N}\right)\right], \tag{15}$$

to the total ring energy from Eq. (12). The comparison is presented in Fig. 4, where the following ration is plotted in dashed line:

$$P_{rn}(N) = \frac{U_R^{nn}(N)}{U_R(N)}100. \tag{16}$$

The discrepancy between two energies behaves similar to the one observed for chains (see Fig. 3, dashed line) and saturates at the value of around 16%. It is also seen that unlike the chain energy, the nearest-neighbor approximation for ideal rings gives an error larger than 10% even for the smallest rings.

C. Embedded rings

The next structures observed in simulations were two embedded rings. Analyzing simulation results, we found that both rings are based on regular polygons (similar to a single ring) with the common center, and the magnetic moments are aligned tangentially, however, the direction of the moments in two rings could be both parallel and antiparallel. In order

to analyze the energy of embedded rings, the analytic expression as a function of ring sizes and the mutual orientation of moments is built below.

The notations adopted in the section are reflected in Fig. 2(c): n is the number of particles in an outer ring, k denotes the number of particles in an inner ring, and R_1 and R_2 are the radii of the inner and outer rings, correspondingly. The angle $\theta \in [0, \ldots, 2\pi/n]$ shows the initial shift of the inner ring from the outer one, ψ is the angle between the polygon side and particle magnetic moment in the inner ring, and, finally, ϕ is the angle analogous to ψ in the outer ring.

The magnetic dipole-dipole interaction between every pair of particles has to be calculated. In order to do that, the functional form of the $U_{dd}(i,j)$ for arbitrary particles i and j is needed. The energy of a single ring is known from Sec. III B, so, the attention will be focused on the interring interaction. Let us introduce a new function l_i,

$$l_i = \left[\left(\frac{2(i-1)\pi}{k} - \theta \right) / \left(\frac{2\pi}{n} \right) \right],$$

where $[\cdot]$ denotes an integer part of the value enclosed in square brackets. The value of the function l_i gives the number of particles from the outer ring which fit into the angle between the first and the ith particle of the inner ring. Thus, the angle between ith particle of the inner ring and the closest particle of the outer ring is given by θ_i,

$$\theta_i = -\frac{2(i-1)\pi}{k} + \theta + \frac{2\pi(l_i+1)}{n}, \quad i \neq 1,$$

with $\theta_1 = \theta$. The number of outer ring particles which belong to the "right" semiplane, restricted by the line based on the displacement vector of the inner ring ith particle [see Fig. 2(c)], can be calculated as follows:

$$p_i = \left[(\pi - \theta_i) / \left(\frac{2\pi}{n} \right) \right] + 1.$$

Here, the square brackets (as above) denote an integer part of the enclosed number. The distance between the inner ring ith particle and the outer ring jth particle is

$$R_j = \left\{ R_1^2 + R_2^2 - 2R_1R_2 \cos\left[\frac{2(j-1)\pi}{n} + \theta_i \right] \right\}^{1/2}.$$

The angle between the magnetic moment of the inner ring ith particle and the displacement vector connecting the inner ring ith particle with outer ring jth particle can be presented in the following conditional form:

$$\psi + \frac{\pi}{2} - \frac{\pi}{k} + \arccos\left(\frac{R_j^2 + R_1^2 - R_2^2}{2R_jR_1} \right) \quad \text{if } i = 1, \ldots, p_i,$$

$$\psi + \frac{\pi}{2} - \frac{\pi}{k} - \arccos\left(\frac{R_j^2 + R_1^2 - R_2^2}{2R_jR_1} \right) \quad \text{if } i = p_i + 1, \ldots, k.$$

The analogous conditional form can be written for the angle between the jth magnetic moment (outer ring) and the ij displacement vector,

$$-\phi - \frac{\pi}{2} + \frac{(2j-1)\pi}{n} + \arccos\left(\frac{R_j^2 + R_1^2 - R_2^2}{2R_jR_1} \right) + \theta_i$$

$$\text{if } i = 1, \ldots, p_i,$$

$$-\phi - \frac{\pi}{2} + \frac{(2j-1)\pi}{n} - \arccos\left(\frac{R_j^2 + R_1^2 - R_2^2}{2R_jR_1} \right) + \theta_i$$

$$\text{if } i = p_i + 1, \ldots, k.$$

The only angle which still has to be defined is the angle between magnetic moments of the inner ring ith particle and outer ring jth particle. Its value also depends on the particle i position,

$$\phi + \psi - \frac{\pi}{k} - \frac{(2j-1)\pi}{n} + \pi - \theta_i \quad \text{if } i = 1, \ldots, p_i,$$

$$-\phi - \psi + \frac{\pi}{k} + \frac{(2j-1)\pi}{n} - \pi + \theta_i \quad \text{if } i = p_i + 1, \ldots, k.$$

Finally, to obtain the total interring magnetic dipole-dipole interaction, we have to sum up all pair interactions,

$$\begin{aligned} U_{ER}^{ir,G} = \frac{m^2}{d^3} \sum_{i=1}^{k} \Bigg[& \sum_{j=1}^{p_i} \frac{1}{R_j^3} \Bigg\{ -\cos\left[\psi + \phi - \frac{\pi}{k} - \frac{(2j-1)\pi}{n} - \theta_i \right] \\ & + 3 \sin\left(A_j - \frac{\pi}{k} + \psi \right) \sin\left[A_j + \frac{(2j-1)\pi}{n} - \phi + \theta_i \right] \Bigg\} \\ & + \sum_{j=p_i+1}^{n} \frac{1}{R_j^3} \Bigg\{ -\cos\left[\psi + \phi - \frac{\pi}{k} - \frac{(2j-1)\pi}{n} - \theta_i \right] \\ & + 3 \sin\left(-A_j - \frac{\pi}{k} + \psi \right) \\ & \times \sin\left[-A_j + \frac{(2j-1)\pi}{n} - \phi + \theta_i \right] \Bigg\} \Bigg], \end{aligned} \tag{17}$$

where $A_j = \arccos[(R_j^2 + R_1^2 - R_2^2)/2R_jR_1]$.

In case of antiparallel orientation of moments in the rings, Eq. (17) can be simplified,

$$\begin{aligned} U_{ER}^{ir} = \frac{m^2}{2d^3} \sum_{i=1}^{k} \sum_{j=1}^{n} \frac{1}{R_j^3} \Bigg\{ & \cos\left(\frac{(2j-2)\pi}{n} + \theta_i \right) \\ & - 3 \cos\left(2A_j + \mathrm{sgn}(p_i - j) \left[\frac{(2j-2)}{n} \pi + \theta_i \right] \right) \Bigg\}. \end{aligned} \tag{18}$$

Here, $\mathrm{sgn}(\cdot)$ is a regular sign function, only it is equal to 1, when the argument is equal to 0. In the case of parallel orientation of the moments in the rings, the interring interaction has the same form as in Eq. (18) but has an opposite sign.

D. Rings side by side

The last structure observed in computer simulations was composed of two rings side by side. In this case, we can also use the energy of single rings so that only the interring interaction has to be calculated. The notations are shown in Fig. 2(d). There are n particles in the left ring, which radius is R_1, and the right ring with radius R_2 contains k particles. There are two mutual shifts of the rings: θ_1 is the initial angle between the displacement vector of the first particle in the left ring and the line, connecting the ring centers, and the analogous angle for the right ring is denoted by θ_2. Similarly to Sec. III C, every particle pair magnetic dipole-dipole interaction has to be calculated. Let ϕ and ψ be the angles between magnetic moment and the polygon side in the left and right rings, respectively. The number of particles in the left ring that are situated above the line which connects ring centers is denoted via $p_1=[(\pi-\theta_1)/(\frac{2\pi}{n})]+1$ and the corresponding value in the right ring is $p_2=[(\pi-\theta_2)/(\frac{2\pi}{k})]+1$. In both expressions square brackets denote an integer part of the enclosed number. It is easy to calculate the angles between ith particle displacement vector in the left ring (jth particle displacement vector in the right ring) and the line which connects ring centers. They are

$$\theta_{1i}=\begin{cases}\dfrac{2(i-1)\pi}{n}+\theta_1 & \text{if } i\le p_1\\ 2\pi-\left(\dfrac{2(i-1)\pi}{n}+\theta_1\right) & \text{if } i>p_1\end{cases}$$

and

$$\theta_{2j}=\begin{cases}\dfrac{2(j-1)\pi}{k}+\theta_2 & \text{if } j\le p_2\\ 2\pi-\left(\dfrac{2(j-1)\pi}{k}+\theta_2\right) & \text{if } j>p_2.\end{cases}$$

The distance between ring centers is a, the distance from the left ring center to the ith particle is l_{1i}, and the corresponding distance calculated for the right ring is l_{2j}. They can be expressed as follows:

$$l_{1i}=(R_1^2+a^2-2R_1a\cos\theta_{1i})^{1/2},$$

$$l_{2j}=(R_2^2+a^2-2R_1a\cos\theta_{2j})^{1/2}.$$

The angle between a and l_{1i} has the form

$$\gamma_i=\arccos\left(\frac{l_{1i}^2+a^2-R_1^2}{2l_{1i}a}\right).$$

These calculations allow us to write down the distance between arbitrary particles i and j from the left and the right rings, respectively,

$$R_{ij}^2=\begin{cases}R_2^2+l_{1i}^2-2R_2l_{1i}\cos(\theta_{2j}-\gamma_i) & \text{if } (i\le p_1 \text{ and } j\le p_2) \text{ or } (i>p_1 \text{ and } j>p_2)\\ R_2^2+l_{1i}^2-2R_2l_{1i}\cos(\theta_{2j}+\gamma_i) & \text{if } (i>p_1 \text{ and } j\le p_2) \text{ or } (i\le p_1 \text{ and } j>p_2).\end{cases}$$

The first condition means that particles i and j are in the same semiplane with respect to the line which connects ring centers; the second expression holds true if the particles are in the different semiplanes with respect to the latter line. The angle between R_{ij} and the radius of the left ring is β_{ij}, and the analogous angle calculated for the right ring is α_{ij}. The angle between the magnetic moment of particle i of the left ring and the vector which connects this particle with particle j in the right ring has a complicated conditional form and is given below:

$$M_{ij}^1=\frac{3\pi}{2}-\beta_{ij}-\frac{\pi}{n}+\phi$$

(i) if particles belong to the same semiplane with respect to the line connecting ring centers and, in addition, if particles lie above this line, the angle between the line and l_{2j} has to be larger than θ_1, but if particles lie below the center-center line, the angle between this line and $i-j$ vector (l_{2j}) should be smaller than θ_1.

(ii) if particles lie in different semiplanes with respect to center-center line and, in addition, if the particle in the left ring is situated below the center-center line, the difference between π and the sum of θ_{1i} with the angle between a and l_{2j} has to be positive; this sum has to be negative otherwise.

Via A_1 the angle between a and l_{2j} is denoted. The above listed conditions can be formalized mathematically,

$$M_{ij}^1 = \begin{cases} \frac{3\pi}{2} - \beta_{ij} - \frac{\pi}{n} + \phi & \text{if } \theta_{1i} - A_1 < 0 \text{ and } i \le p_1 \text{ and } j \le p_2 \\ \frac{3\pi}{2} - \beta_{ij} - \frac{\pi}{n} + \phi & \text{if } \pi - \theta_{1i} - A_1 \ge 0 \text{ and } i > p_1 \text{ and } j \le p_2 \\ \frac{3\pi}{2} - \beta_{ij} - \frac{\pi}{n} + \phi & \text{if } \pi - \theta_{1i} - A_1 < 0 \text{ and } i \le p_1 \text{ and } j > p_2 \\ \frac{3\pi}{2} - \beta_{ij} - \frac{\pi}{n} + \phi & \text{if } \theta_{1i} - A_1 \ge 0 \text{ and } i > p_1 \text{ and } j > p_2 \\ -\frac{\pi}{2} + \beta_{ij} - \frac{\pi}{n} + \phi & \text{if } \theta_{1i} - A_1 \ge 0 \text{ and } i \le p_1 \text{ and } j \le p_2 \\ -\frac{\pi}{2} + \beta_{ij} - \frac{\pi}{n} + \phi & \text{if } \pi - \theta_{1i} - A_1 < 0 \text{ and } i > p_1 \text{ and } j \le p_2 \\ -\frac{\pi}{2} + \beta_{ij} - \frac{\pi}{n} + \phi & \text{if } \pi - \theta_{1i} - A_1 \ge 0 \text{ and } i \le p_1 \text{ and } j > p_2 \\ -\frac{\pi}{2} + \beta_{ij} - \frac{\pi}{n} + \phi & \text{if } \theta_{1i} - A_1 < 0 \text{ and } i > p_1 \text{ and } j > p_2. \end{cases}$$

Introducing A_2 as the angle between a and l_{1i}, the expression for M_{ij}^2 (which stands for the angle between the magnetic moment of jth particle of the right ring and $i-j$ vector) can be obtained in the following conditional form:

$$M_{ij}^2 = \begin{cases} \frac{3\pi}{2} - \alpha_{ij} + \frac{\pi}{k} - \psi & \text{if } \theta_{2j} - A_2 < 0 \text{ and } i \le p_1 \text{ and } j \le p_2 \\ \frac{3\pi}{2} - \alpha_{ij} + \frac{\pi}{k} - \psi & \text{if } \pi - \theta_{2j} - A_2 < 0 \text{ and } i > p_1 \text{ and } j \le p_2 \\ \frac{3\pi}{2} - \alpha_{ij} + \frac{\pi}{k} - \psi & \text{if } \pi - \theta_{2j} - A_2 \ge 0 \text{ and } i \le p_1 \text{ and } j > p_2 \\ \frac{3\pi}{2} - \alpha_{ij} + \frac{\pi}{k} - \psi & \text{if } \theta_{2j} - A_2 \ge 0 \text{ and } i > p_1 \text{ and } j > p_2 \\ -\frac{\pi}{2} + \alpha_{ij} + \frac{\pi}{k} - \psi & \text{if } \theta_{2j} - A_2 \ge 0 \text{ and } i \le p_1 \text{ and } j \le p_2 \\ -\frac{\pi}{2} + \alpha_{ij} + \frac{\pi}{k} - \psi & \text{if } \pi - \theta_{2j} - A_2 \ge 0 \text{ and } i > p_1 \text{ and } j \le p_2 \\ -\frac{\pi}{2} + \alpha_{ij} + \frac{\pi}{k} - \psi & \text{if } \pi - \theta_{2j} - A_2 < 0 \text{ and } i \le p_1 \text{ and } j > p_2 \\ -\frac{\pi}{2} + \alpha_{ij} + \frac{\pi}{k} - \psi & \text{if } \theta_{2j} - A_2 < 0 \text{ and } i > p_1 \text{ and } j > p_2. \end{cases}$$

The values of ϕ and ψ in case of ideal rings, whose magnetic moments are aligned tangentially to the circles on which the ideal rings are based, can be written as $\phi = \pi/n$ and $\psi = \pi/k$. In this case, magnetic moments of the closest particles [see Fig. 2(d), particle filled with gray] are antiparallel. By adding π to one of the angles (ϕ or ψ), the orientation of magnetic moments in two rings side by side might be switched to the parallel one, and the interring interaction energy changes the sign.

Using the notations listed above, the angle between magnetic moments of ith and jth particles is the sum $M_{ij} = M_{ij}^1 + M_{ij}^2$.

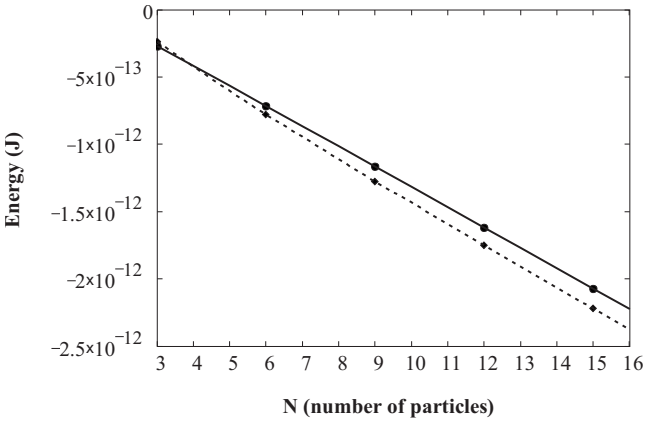

FIG. 5. Energy of the structure (in Joules, for 10 nm particles made of magnetite). Theoretical curves: solid line—chain energy; dashed line—ring energy. Simulation data: circles and rhombuses for a chain and a ring, respectively.

Finally, the interring energy can be calculated as

$$U_{SR}^{G} = \frac{m^2}{d^3} \sum_{j=1}^{k} \left[\sum_{i=1}^{n} \frac{1}{R_{ij}^3} (\cos M_{ij} - 3 \cos M_{ij}^1 \cos M_{ij}^2) \right]. \tag{19}$$

Having obtained the complete set of energies, we proceed with comparing them and studying the peculiarities of different structures.

IV. COMPARISON OF DIFFERENT GROUND STATE STRUCTURES

In the previous sections we identified structures that might fulfill the ground state of a ferroparticle monolayer. They were a chain, a single ring, two embedded rings, and two rings side by side. We also calculated analytically the minimum energies of these structures. The final steps of this study are to compare the energies and to make a profound conclusion on the ground state structure. In this section, when the values of energies are provided in Joules, the reference model ferrofluid is composed of 10 nm magnetite particles with the saturation magnetization of the bulk equal to 480 kA/m.

The comparison starts with Fig. 5, where the energies (in Joules) of a rigid rodlike chain (solid line) and of an ideal ring (dashed line) are plotted as functions of particle number N. Up to four particles, the chain is energetically preferable to a ring, then, the curves intersect, the ring becomes more advantageous, and the energies keep decreasing linearly with N, preserving a constant difference. The value of this difference, namely, $3m^2\pi^2/d^3$, can be found easily from Eqs. (5) and (13). Open symbols in this figure correspond to the results of simulations and are indistinguishable from the theoretical results: circles are obtained for a chain; rhombuses represent a ring. At this stage (for systems larger than four particles), the chain is to be excluded from consideration as a candidate for the ground state topology.

In Fig. 6 we present the relative energy of two embedded rings as a function of k/N (the number of particles in an inner ring divided by the number of particles in both rings). As a zero level in this plot we take the energy of a single ring made of N particles and normalize embedded ring energy by its value for $k=3$. Here, four different curves are plotted and compared to the results of simulations: solid line (theory) and circles (simulations) describe embedded rings with the total number of particles $N=25$; dashed line (theory) and rhombuses show the energy for $N=36$; $N=49$ is given by theoretical dashed-dotted line and simulation squares; and to plot the energy for $N=100$ we use dotted line (theory) and triangles (simulations). All curves (together with symbols) show the same universal behavior. Starting obviously from zero, they grow rapidly to create a very high potential barrier for $k=3$ and then go to zero up to $k/N \sim 0.42$, where we observe a sharp jump. This ratio goes to 1/2 (with growing N) and corresponds to the close contact of inner and outer rings, meaning that the barrier is caused by the steric repulsion simply. However, the energy keeps decreasing when the rings approach the close contact. Let us investigate the interring interaction in detail. We have shown that the mutual orientation of moments changes the sign of the interring energy from minus (antiparallel orientation) to plus (parallel orientation). The point is this flip does not affect the total energy strongly, as the interring interaction energy value is approximately 100 times smaller than the sum of interaction energies inside both rings. Thus, for example, for embedded rings made of 18 particles with 6 particles in the inner ring (which is the most advantageous configuration for the embedded rings of 18 particles), for antiparallel alignment of moments the total reduced (i.e., divided by $2m^2/d^3$) energy of two embedded rings is −40.45; within this energy the interring energy contribution has the value of −0.39. In case of parallel orientation of magnetic moments in embedded rings, these reduced energies are correspondingly −39.68 and 0.39. Besides being small, the interring interaction depends strongly on the ratio of particles in the inner and outer rings.

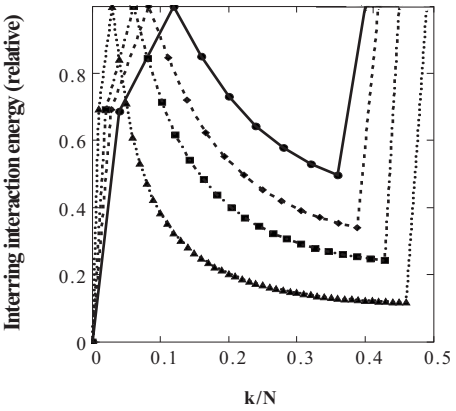

FIG. 6. The relative energy of two embedded rings as a function of k/N. As a zero level the energy of a single ring made of N particles is taken. The energy is normalized by its value for $k=3$. Solid line (theory) and circles (simulations) describe embedded rings with the total number of particles $N=25$; dashed line (theory) and rhombuses show the energy for $N=36$; $N=49$ is given by theoretical dashed-dotted line and simulation squares; and to plot the energy for $N=100$ we use dotted line (theory) and triangles (simulations).

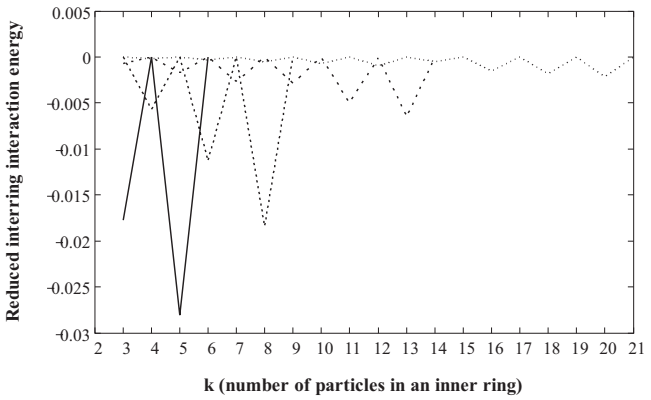

FIG. 7. Reduced interring interaction energy for different N versus the number of particles in an inner ring (k). Solid line corresponds to $N=20$, dashed line depicts the interring interaction for the system with $N=25$, and dashed-dotted and dotted lines describe the latter interaction for embedded rings composed by $N=36$ and $N=49$ particles, respectively. Only the theoretical data are presented.

Thus, it is different from zero for particular ratios only. We plot the reduced interring interaction for different N (total number of particles in both rings) in Fig. 7. All curves are plotted versus the number of particles in an inner ring (k). We present theoretical curves only to avoid the overloading of the picture; simulation data for this plot agree with our theory. Solid line corresponds to $N=20$, dashed line depicts the interring interaction for the system with $N=25$, and dashed-dotted and dotted lines describe the latter interaction for embedded rings composed of $N=36$ and $N=49$ particles, respectively. This sawlike shape can be explained in terms of symmetry compensation of pair interactions. When the symmetry is broken, we observe a nonzero interaction. It is worth saying that when N goes to infinity, plots in Figs. 6 and 7 do not give an irrefragable answer to the main question of the comparison, namely, we cannot conclude whether the energies of embedded rings coincide (become lower) with (than) the energy of a single ideal ring. To clarify this point, we evaluated analytically the limit,

$$\lim_{N\to\infty}\{U_R(N)-[U_R(n)+U_R(k)+U_{ER}^{ir}]\}=-\lim_{N\to\infty}U_{ER}^{ir}, \tag{20}$$

where $n+k=N$. The inequality $U_{ER}^{ir}>0$ if holds true for any N, means that a single ring has the energy lower than the one of two embedded rings. It is not needed, though, to construct the estimate for the complete expression of U_{ER}^{ir} because the interaction of the inner ring (radius R_1) particles with the particles from outer ring (radius R_2) is symmetric. So, without loss of generality, we can take into account the interaction between one randomly chosen particle from the inner ring with every particle from the outer ring. One can notice that the sum from Eq. (18) has the following property: except for the first term which is negative, the sum of terms with indices j and $n+2-j$ for $j\geq 2$ is positive. Thus, it is sufficient to find at least one combination of such terms which compensates the negative contribution of the first one. The sufficient condition will vary slightly for odd and even n

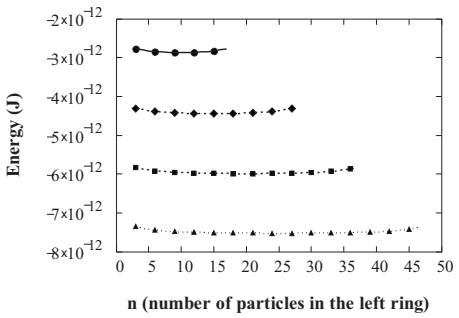

FIG. 8. The energy (in Joules, for 10 nm particles made of magnetite) of two rings side by side versus the number of particles in the left ring. Solid line (theory) and circles (simulations) correspond to $N=20$; dashed line (theory) and rhombuses (simulations) depict the energy of the rings side by side for the system with $N=30$; and dashed-dotted (theory) with squares (simulations) and dotted (theory) with triangles (simulations) lines describe the latter total energy for $N=40$ and $N=50$ particles, respectively.

(number of particles in an outer ring, here, we used the notations adopted in Sec. III C),

$$\sin(A_j)\leq 1-\frac{R_j^3}{2(R_2-R_1)^3} \quad \text{if } n \text{ is odd},$$

$$\sin(A_j)\leq 1-\frac{R_j^3}{2(R_2-R_1)^3}+\frac{R_j^3}{2(R_2+R_1)^3} \quad \text{if } n \text{ is even}. \tag{21}$$

Both conditions can be fulfilled if, for example, the term with index $j=2$ is taken. It means that the energy of embedded rings is always higher than the energy of a single ring, but the point is, that once the embedded rings are formed in simulations, they have to overcome a very high energy barrier to become a single ring, so very long simulations are needed to rich the single ring structure.

To verify finally the ground state structure of a monodisperse ferrofluid monolayer, we have to analyze the last structure, namely, two rings situated side by side. It is obvious that two rings try to be as close as possible to each other. In this case they guarantee the optimum for the dipolar interactions between particles in different rings by means of reducing the distance. In Fig. 8, we plot the energy (in Joules) of two rings side by side versus the number of particles in the left ring. Solid line (theory) and circles (simulations) correspond to $N=20$; dashed line (theory) and rhombuses (simulations) depict the energy of the rings side by side for the system with $N=30$; and dashed-dotted (theory) with squares (simulations) and dotted (theory) with triangles (simulations) lines describe the latter total energy for $N=40$ and $N=50$ particles, respectively. It is clearly seen that rings side by side try to make the number of particles in the right and left rings equal. The detailed analysis of the interring interaction is provided in Table I with configurations of neighboring particles given in Fig. 9.

In Table I the reduced energy is presented for $N=20$ and $n=10$ (number of particles in the left ring). The top line in Table I contains numbers of configurations given in Fig. 9.

TABLE I. Values of reduced energies for rings side by side [see Eqs. (12) and (19)].

Conf.	I	II	III	IV	V	VI
$U_{SR}(20)+2U_R(10)$	−45.16	−45.73	−45.71	−45.18	−45.18	−45.71
$U_{SR}(20)$	0.28	−0.28	−0.27	0.27	0.26	−0.26

The lowest possible energy of rings side by side corresponds to the antiparallel orientation of moments (II, third column, Table I) when the closest particles are side by side. Even for this configuration the total energy (second line, Table I) is approximately 200 times lower than the interring interaction (third line, Table I). So, similarly to the case of the embedded rings, the interring interaction of two rings side by side is extremely weak, but it is never zero. The latter fact can be shown analogously to the case of embedded rings; we do not provide this proof here.

To make the picture complete, we plot the energies of the most advantageous structures from each class divided by the energy of an ideal ring as a function of the total number of particles N in Fig. 10. The energy ratio for an ideal rodlike chain is plotted with solid line (theory) and circles (simulations). The value of unity for an ideal ring is depicted by dashed line. Squares together with dashed-dotted line show the energy ratio for embedded rings at close contact with antiparallel orientation of magnetic moments. The energy ratio for two rings side by side in configuration II (see Fig. 9 and Table I) is presented with theoretical dotted line, and triangles represent simulation data. Thus, the single ring is the ground state structure in a ferrofluid monolayer. However, both embedded rings and rings side by side provide very close but anyway local minima of the energy. As for the chains, they appear to be a ground state structure for systems composed of three and less particles (see Fig. 5).

V. CONCLUSION

By means of Monte Carlo simulations, taking into account the magnetic dipole-dipole interaction between all particles in the system, we found different topological structures which are likely to exist at low temperatures in monolayers: chains, rings, embedded rings, and rings side by side. Our simulations demonstrated that at low temperatures the particle magnetic moments fluctuated predominantly within the plane of the monolayer. Additionally, rings were proved to be based on regular polygons. The reduction in spatial degrees of freedom made an analytical treatment possible by which we computed and minimized analytically the energy of each structure from the list above. At low temperatures, predictably, the minimal energy configuration for the chain is the rodlike configuration of moments, and for an ideal ring the minimal energy configuration corresponds to the tangential alignment of particle magnetic moments. Both, for chains and rings, the energies decrease linearly with the number of particles. Looking at the asymptotic behavior one can conclude the following:

(i) The approximation of only considering nearest neighbors is valid for calculating chain energies. The precision of the latter approximation is higher than 5% for chains shorter than 5; for industrial ferrofluids particles are usually 10–15 nm in diameter and, if aggregating, form chains of length 2–4, which support the approximation of the nearest-neighbor interaction. However, the same nearest-neighbor approach fails to describe the energy of a ring.

(ii) The ring becomes the energetically favorable configuration for systems larger than four particles. When the total number of particles in a system is large enough, the difference between chain and ring energies becomes constant and equals $3m^2\pi^2/d^3$.

Our theoretical investigations supported by the results of computer simulations of embedded rings and rings side by side revealed several peculiarities:

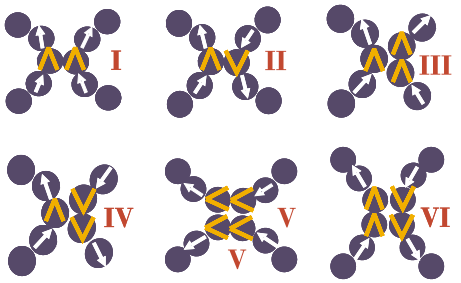

FIG. 9. (Color online) Possible configurations of neighboring particles in the rings side by side. Corresponding energies are presented in Table I. Configurations are numbered in the legend with Roman numerals from I to VI.

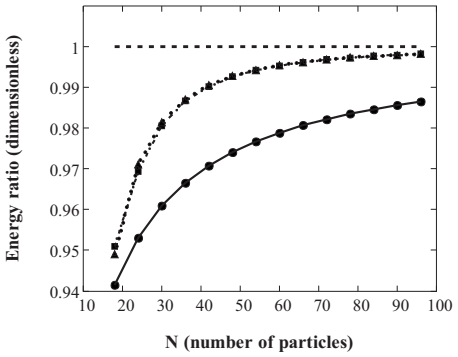

FIG. 10. Energy ratios (the energy of the structure divided by the energy of an ideal ring) of the most favored structures from each class as a function of the total number of particles N. The ratio for an ideal rodlike chain is plotted with solid line (theory) and circles (simulations). The ratio for an ideal ring (namely, exact unity) is depicted by dashed line. Squares together with dashed-dotted line show the ratio for embedded rings at close contact with antiparallel orientation of magnetic moments. The ratio for two rings side by side in configuration II (see Fig. 9 and Table I) is presented with the theoretical line and triangles represent simulation data.

(i) Rings in the latter structures tend to be as close as possible to each other. Two rings side by side have the same size, and in embedded rings the inner ring contains the largest number of particles possible.

(ii) The energies of embedded rings and rings side by side are very close to the energy of an ideal ring but remain higher even in the limiting case (when the number of particles goes to infinity). This proximity explains why those structures once formed in simulations are extremely stable. The other reason to observe these structures in simulations is the potential barrier which embedded rings have to overcome to collapse into a single ring (see Fig. 6). This very potential barrier probably led the authors of the work [37] to conclusion that embedded rings were the most probable structures for large coupling constants and large numbers of particles. On the other hand, here we study the ground state, where, unlike the abovementioned work [37], entropy does not play any part. Thus, for large coupling constants we believe our findings to be valid.

(iii) The absolute values of inter-ring interactions in both structures are two orders of magnitude lower than the values of the total energies. The inter-ring energy minima are always reached for the antiparallel orientation of magnetic moments.

The combination of computer simulations and analytical studies proved that the ideal single ring is the ground state structure for identical magnetic particles in a monolayer. For less than four particles the ground state structure is the rodlike chain. For these conclusions it is important that the plane of monolayer is infinite in our model, i.e., concentration dependencies are not considered here.

Computer experiments, besides helping to classify the structures and verify theoretical results, put forward several recommendations for simulated annealing. Repeating our simulations, we found that there was a certain temperature interval $T_H, \ldots, T_L$, $T_H > T_L$ for which the equilibration proceeded efficiently and whose structures exerted a crucial influence on the structure observed at lower temperatures. Basically, no matter how fast the temperature was lowered before reaching a certain value ($T > T_H$), it did not influence the resulted structure nor the latter structure depended on the procedure for temperatures below that region ($T < T_L$). In other words, structures formed within this temperature range would remain the same even if further simulations are very long. The physical reason for the latter temperature interval to exist is clear: above T_H the dipolar interactions are too weak to hold the structures, below T_L the fluctuations are too low to move the system from the local (absolute) minimum of the energy. To determine T_H and T_L an additional computer experiment was carried out. We took the ideal structures (a rodlike chain, a ring, embedded rings, and rings side by side) at very low temperatures (in our simulations it corresponded to the value of coupling constant $m^2/kT \sim 64$) and started to heat the system up. The chain of 64 particles (the structure known to have the energy higher than a ring) folded to a ring (the ground state structure) at $m^2/kT \sim 10$. Further heating destroyed the ring at $m^2/kT \sim 5$. Thus, the most important interval for simulated annealing of monodisperse magnetic dipoles in the plain is roughly given by m^2/kT range [5,10], which for magnetite 10 nm particle corresponds to $T_H \sim 90$ K and $T_L \sim 45$ K (in comparison, for magnetite particles of 18 nm with 2 nm nonmagnetic layer this interval is $T_H \sim 260$ K and $T_L \sim 140$ K). In nearly the same m^2/kT range (see Fig. 1) the fluctuations of magnetic moments in the out of plain direction drop abruptly. This temperature interval has to be handled with the highest precision. The existence of this temperature range allows us to reduce the computational time by one order of magnitude. The final recommendation proposed here is the following: if there are initial configurations that are likely candidates for the ground states, it is much faster to heat the system first and to find the interesting temperature interval; a further analysis can be safely carried out for this interval only.

The ability to perform exact analytical energy minimization on configurations relied on the absence of the third spatial dimension, meaning in three dimensions it will be probably impossible to carry out the same procedure. A simplification adopted in the present work is the monodispersity of our suspension and the absence of an external magnetic field which are not addressed in this paper. These problems will be addressed in future investigations, and we believe that the method of ground state structure analysis proposed in the present paper will serve as a helpful tool for future investigations.

ACKNOWLEDGMENTS

This research was carried out with the financial support of DFG-RFBR Grant No. HO 1108/12-1. One of the authors (S.S.K.) was supported by the grant of President RF under Grant No. MK-412.2008.2. The research was partially supported by RFBR Grant No. 08-02-00647 and CRDF Grant No. PG07-005-02.

[1] E. L. Resler and R. E. Rosensweig, AIAA J. **2**, 1418 (1964).
[2] E. Blum, M. M. Maiorov, and A. Cebers, *Magnetic Fluids* (Walter de Gruyter, Berlin, 1997).
[3] Ch. Alexiou *et al.*, J. Drug Target. **11**, 139 (2003).
[4] I. Hilger *et al.*, in *Inorganic Materials, Recent Advances*, edited by D. Bahadur, S. Vitta, and O. Prakash (Narosa, New Delhi, 2004).
[5] P. G. de Gennes and P. A. Pincus, Phys. Kondens. Mater. **11**, 189 (1970).
[6] P. C. Jordan, Mol. Phys. **25**, 961 (1973).
[7] M. A. Osipov, P. I. C. Teixeira, and M. M. Telo da Gama, Phys. Rev. E **54**, 2597 (1996).
[8] A. Yu. Zubarev and L. Yu. Iskakova, J. Exp. Theor. Phys. **80**, 857 (1995).
[9] J. M. Tavares, M. M. Telo da Gama, and M. A. Osipov, Phys. Rev. E **56**, R6252 (1997).

[10] J. M. Tavares, J. J. Weis, and M. M. Telo da Gama, Phys. Rev. E **59**, 4388 (1999).
[11] R. van Roij, Phys. Rev. Lett. **76**, 3348 (1996).
[12] T. Tlusty and S. A. Safran, Science **290**, 1328 (2000).
[13] K. I. Morozov and M. I. Shliomis, in *Ferrofluids, Magnetically Controllable Fluids and Their Applications*, Lecture Notes in Physics, edited by S. Odenbach (Springer-Verlag, Berlin, 2002).
[14] V. S. Mendelev and A. O. Ivanov, Phys. Rev. E **70**, 051502 (2004).
[15] A. O. Ivanov, Z. Wang, and C. Holm, Phys. Rev. E **69**, 031206 (2004).
[16] J. J. Weis and D. Levesque, Phys. Rev. Lett. **71**, 2729 (1993).
[17] D. Levesque and J. J. Weis, Phys. Rev. E **49**, 5131 (1994).
[18] P. Jund, S. G. Kim, D. Tomanek, and J. Hetherington, Phys. Rev. Lett. **74**, 3049 (1995).
[19] P. J. Camp and G. N. Patey, Phys. Rev. E **62**, 5403 (2000).
[20] A. F. Pshenichnikov and V. Mekhonoshin, J. Magn. Magn. Mater. **213**, 357 (2000).
[21] Z. Wang, C. Holm, and H. W. Müller, Phys. Rev. E **66**, 021405 (2002).
[22] Z. Wang and C. Holm, Phys. Rev. E **68**, 041401 (2003).
[23] J. J. Weis, J. M. Tavares, and M. M. Telo da Gama, J. Phys.: Condens. Matter **14**, 9171 (2002).
[24] J. J. Weis, J. Phys.: Condens. Matter **15**, S1471 (2003).
[25] M. Aoshima and A. Satoh, J. Colloid Interface Sci. **280**, 83 (2004).
[26] T. Kristóf and I. Szalai, Phys. Rev. E **72**, 041105 (2005).
[27] J. M. Tavares, J. J. Weis, and M. M. Telo da Gama, Phys. Rev. E **73**, 041507 (2006).
[28] P. D. Duncan and P. J. Camp, Phys. Rev. Lett. **97**, 107202 (2006).
[29] C. Holm *et al.*, J. Phys.: Condens. Matter **18**, S2737 (2006).
[30] W. Wen, F. Kun, K. F. Pal, D. W. Zheng, and K. N. Tu, Phys. Rev. E **59**, R4758 (1999).
[31] V. F. Puntes, K. M. Krishnan, and A. P. Alivisatos, Science **291**, 2115 (2001).
[32] K. Butter *et al.*, J. Phys.: Condens. Matter **15**, S1451 (2003).
[33] M. Klokkenburg *et al.*, Phys. Rev. Lett. **96**, 037203 (2006).
[34] S. Kantorovich, J. J. Cerda, and C. Holm, Phys. Chem. Chem. Phys. **10**, 1883 (2008).
[35] D. Tománek *et al.*, Z. Phys. D: At., Mol. Clusters **40**, 539 (1997).
[36] F. Kun, W. Wen, K. F. Pal, and K. N. Tu, Phys. Rev. E **64**, 061503 (2001).
[37] H. Morimoto, T. Maekawa, and Y. Matsumoto, Phys. Rev. E **68**, 061505 (2003).
[38] X. Chen *et al.*, Chin. Phys. Lett. **22**, 486 (1995).
[39] Yu. A. Koksharov *et al.*, Thin Solid Films **515**, 731 (2006).
[40] J. D. Weeks, D. Chandler, and H. C. Andersen, J. Chem. Phys. **54**, 5237 (1971).
[41] N. Metropolis *et al.*, J. Chem. Phys. **21**, 1087 (1953).
[42] S. S. Kantorovich, J. Magn. Magn. Mater. **289**, 203 (2005).